

Plasmons due to the Interplay of Dirac and Schrödinger Fermions

Stefan Juergens, Paolo Michetti, and Björn Trauzettel

Institute of Theoretical Physics and Astrophysics, University of Würzburg, D-97074 Würzburg, Germany

(Received 23 September 2013; published 21 February 2014)

We study the interplay between Dirac and Schrödinger fermions in the polarization properties of a two-dimensional electron gas (2DEG). Specifically, we analyze the low-energy sector of narrow-gap semiconductors described by a two-band Kane model. In the context of quantum spin Hall insulators, particularly, in Hg(Cd)Te quantum wells, this model is named the Bernevig-Hughes-Zhang model. Interestingly, it describes electrons with intermediate properties between Dirac and Schrödinger fermions. We calculate the dynamical dielectric function of such a model at zero temperature within random phase approximation. Surprisingly, plasmon resonances are found in the intrinsic (undoped) limit, whereas they are absent—in that limit—in graphene as well as ordinary 2DEGs. Additionally, we demonstrate that the optical conductivity offers a quantitative way to identify the topological phase of Hg(Cd)Te quantum wells from a bulk measurement.

DOI: [10.1103/PhysRevLett.112.076804](https://doi.org/10.1103/PhysRevLett.112.076804)

PACS numbers: 73.21.Fg, 71.45.Gm, 71.45.Lr, 77.22.Ch

Introduction.—The advent of graphene [1] has paved the way to the investigation of Dirac fermions in condensed matter systems [2]. Since then, Dirac fermion physics has also been analyzed in many other two-dimensional (2D) systems. Prominent examples are the surface states of 3D topological insulators (TIs) [3,4], where the helicity, i.e., coupling of momentum and spin degrees of freedom, introduces new interesting phenomena [5,6]. Another rich system is offered by the bulk bands of the 2D TI phase in Hg(Cd)Te quantum wells [7], described by the Bernevig-Hughes-Zhang (BHZ) model [8], where the interplay of Dirac and Schrödinger fermion physics can be studied in combination with topology [9].

An important aspect of condensed matter physics is the influence of Coulomb interaction on observables. In the Dirac fermion system graphene, this research has been intensified in recent years [10–15], resulting even in the development of plasmon technology [16,17]. Plasmons are collective density oscillations commonly occurring at finite doping in an electronic system. Plasmons in Dirac fermion systems have been experimentally observed in graphene [18–20] as well as 3D TIs [21]. Usually absent in the undoped limit, intrinsic plasmons have been predicted in graphene, when the electron and hole gas have a finite density due to thermal excitations [22,23], or with the inclusion of excitonic effects through ladder-type vertex corrections in the calculation of the dielectric response function [24]. Yet, the latter result is still under debate due to the neglect of diagrams of the same order [25]. Interestingly, a reduction of the dimension to 1D gives rise to intrinsic plasmons in metallic armchair nanoribbons [26]. These situations are physically distinct from our prediction below where we show that plasmons, in the intrinsic limit, can appear due to an interplay of Dirac and Schrödinger physics.

We present a calculation of the dielectric properties of the BHZ model at zero temperature and doping, within random phase approximation (RPA). Surprisingly, the interpolating character of the model gives rise to plasmonic resonances, absent in both limiting cases of Dirac and two-dimensional electron gas (2DEG) system. We discuss their presence and damping rate for various parameters, including the TI and the normal insulator (NI) phase as well as experimentally realistic values. Furthermore, we calculate the bulk optical conductivity, which offers a way to quantitatively resolve between NI and TI phase.

Model.—The BHZ model for fermions in Hg(Cd)Te quantum wells—near the Γ point in the Brillouin zone—has the following form [8]:

$$H = \begin{pmatrix} h(\mathbf{k}) & 0 \\ 0 & h^*(-\mathbf{k}) \end{pmatrix},$$

$$h(\mathbf{k}) = V(k) + \mathbf{d}_k \cdot \vec{\sigma},$$

$$\mathbf{d}_k = (Ak_x, Ak_y, M(k)), \quad (1)$$

where $\vec{\sigma}$ are the Pauli matrices associated with the band-pseudospin degree of freedom (subband E_1 or H_1 in HgTe quantum wells), $V(k) = C - Dk^2$, and $M(k) = M - Bk^2$. The system possesses time-reversal symmetry and H is block diagonal in the Kramers partner or spin degree of freedom. Therefore, we restrict ourselves to the block $h(\mathbf{k})$, from which the results can be extended to the other one by applying the time-reversal operator.

Evidently, $h(\mathbf{k})$ smoothly interpolates, as a function of its parameters, between a Dirac and a conventional 2DEG system. The off-diagonal term (A parameter) is typical of a Dirac system with M the Dirac mass. Negative masses correspond to the TI phase described by a finite \mathbb{Z}_2

topological invariant [27], while positive masses lead to a normal insulator (assuming $B < 0$). In analogy to a 2DEG, the diagonal parts bear kinetic energy elements which preserve (B parameter) and break (D parameter) particle-hole symmetry. The eigenstates of Eq. (1) are characterized by energy dispersion and pseudospin [28]:

$$E_{k,\lambda} = V(k) + \lambda|\mathbf{d}_k|, \quad (2)$$

$$\langle \mathbf{k}, \lambda | \vec{\sigma} | \mathbf{k}, \lambda \rangle = \lambda \hat{\mathbf{d}}_k, \quad (3)$$

with $\lambda = \pm$ for conduction and valence bands, where $\hat{\mathbf{d}}$ is the direction of the \mathbf{d} vector, illustrated in Fig. 1.

Polarization function.—At zero doping, there are no extrinsic parameters like the Fermi momentum. Nevertheless, the parameters of the BHZ model provide natural units for the wave vector $q_0 = A/|B|$ and the energy $E_0 = Aq_0$. We define the dimensionless wave vector $\mathbf{X} = \mathbf{q}/q_0$ and frequency $\Omega = \hbar\omega/E_0$, as well as the dimensionless parameters $\xi_M = M/E_0$ and $\xi_D = D/|B|$. Hence, the physical scales of momentum and energy are fixed by the ratio of the A parameter (linked to the Dirac physics) to the B parameter (linked to the 2DEG physics). In terms of the dimensionless variables, we expect, therefore, an intermediate behavior for $X \sim 1$, while for $X, \Omega \rightarrow 0$ ($X, \Omega \rightarrow \infty$), the Dirac (2DEG) physics should emerge.

The linear response of a homogeneous system to an external applied potential is described by the polarization function $\Pi^R(\mathbf{q}, \omega)$. This response comprises the two main phenomena of screening and dissipation, included in the real and imaginary part of $\Pi^R(\mathbf{q}, \omega)$, respectively. The intrinsic polarization function of the BHZ model in RPA approximation at zero temperature, where only interband terms contribute, can be written as

$$\Pi^R(X, \Omega) = \frac{g_s}{|B|} \sum_{\lambda=\pm} \int \frac{d^2\tilde{\mathbf{X}}}{(2\pi)^2} \frac{\lambda \mathcal{F}(\tilde{\mathbf{X}}, \tilde{\mathbf{X}}')}{\Omega + i0^+ + \epsilon_{\tilde{\mathbf{X}},-\lambda} - \epsilon_{\tilde{\mathbf{X}}',\lambda}}, \quad (4)$$

with $\tilde{\mathbf{X}}' = \tilde{\mathbf{X}} + \mathbf{X}$, 0^+ a positive infinitesimal, $g_s = 2$ for spin degeneracy, $\epsilon_{\tilde{\mathbf{X}},\lambda} = E_{q_0\tilde{\mathbf{X}},\lambda}/E_0$ the dimensionless eigenenergies, and

$$\mathcal{F}(\mathbf{X}, \mathbf{X}') = |\langle \mathbf{k}, + | \mathbf{k}', - \rangle|^2 = \frac{1}{2} [1 - \hat{\mathbf{d}}_{q_0\mathbf{X}} \cdot \hat{\mathbf{d}}_{q_0\mathbf{X}'}]. \quad (5)$$

From Eq. (4), we see that $|B|\Pi^R(X, \Omega)$ is a function of X and Ω , while it parametrically depends on ξ_M and ξ_D .

The same is also true for the dynamical dielectric function, which acquires the form

$$\frac{\epsilon(X, \Omega)}{\epsilon_r} = 1 - \alpha g(X, \Omega), \quad (6)$$

where we define the effective fine-structure constant $\alpha = e^2/(4\pi\epsilon_0\epsilon_r A)$ [15]. In graphene, it is of the order $\alpha = 2.2/\epsilon_r$ [16]; in HgTe, one finds $\alpha \approx 4/\epsilon_r$ [9,29]. Here, ϵ_r is the background dielectric constant and we introduce the function $g(X, \Omega) = (2\pi|B|/X)\Pi^R(X, \Omega)$. While ϵ_r accounts for the screening of internal electronic shells, $-\alpha g(X, \Omega)$ yields the dynamical screening due to valence electrons within RPA.

Besides the screening properties, the dielectric function also provides insight into the excitations of the system. Zeros of $\epsilon(X, \Omega)$ identify momentum and frequency at which the system allows for self-sustaining density perturbations, which form collective excited modes of the system, i.e., plasmons. The dispersion relation of the plasmonic solutions is obtained by solving [30,31]

$$\epsilon(X, \Omega_p - i\Gamma) = 0, \quad (7)$$

where Ω_p is the dimensionless eigenfrequency of the plasmon and the finite imaginary part $\Gamma = \gamma/E_0$ accounts for the possible damping due to single-particle excitations.

Dissipation processes in the interacting system are described by ϵ through the loss function

$$\text{Im} \left[-\frac{1}{\epsilon} \right] = \frac{1}{\epsilon_r \alpha} \frac{\text{Im}[g(X, \Omega)]}{|\frac{1}{\alpha} - g(X, \Omega)|^2}, \quad (8)$$

which accounts for the excitation of both single-particle electron-hole pairs and collective plasmon modes.

Overlap factor.—Massless Dirac fermions (corresponding to $D = B = M = 0$) are characterized by their helicity and, consequently, the overlap factor reduces to $\mathcal{F}(\mathbf{k}, \mathbf{k}') = (1 - \cos\theta)/2$, with θ the angle between \mathbf{k} and \mathbf{k}' . Hence, it is strictly one (zero) for \mathbf{k} and \mathbf{k}' pointing in the opposite (same) direction. Eigenstates of the BHZ model are characterized by their pseudospin. The quadratic terms turn the pseudospin out of plane in opposite

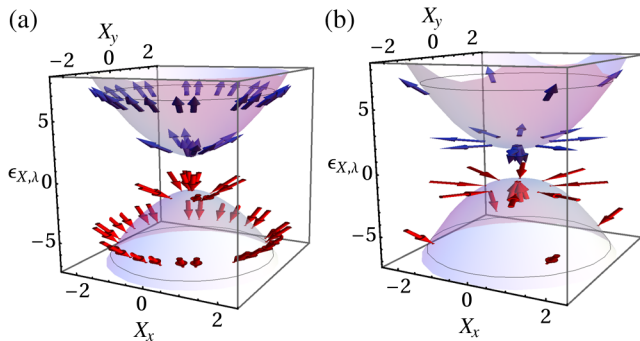


FIG. 1 (color online). Dispersion relation and pseudospin properties of the eigenstates of the BHZ model for a NI phase with $\xi_M = 1/2$ (a) and TI phase with $\xi_M = -1/2$ (b). The two bands have been artificially separated by an additional $2\epsilon_{X,\lambda}$ for a better illustration of the pseudospin.

directions for conduction and valence bands at large X ; see Fig. 1. This behavior results in a decay of the overlap factor for $A \rightarrow 0$ or $X \rightarrow \infty$, reproducing the limit of a conventional 2DEG system where intrinsic polarization is absent. For $X \ll |\xi_M|$, a finite Dirac mass term turns the pseudospin out of plane as well, in the same direction as the quadratic terms [Fig. 1(a)] for $M > 0$ (NI phase) or in the opposite direction [Fig. 1(b)] for $M < 0$ (TI phase). This behavior suppresses the overlap factor. In the TI phase, valence and conduction band states with unitary overlap can always be found for finite X . Thus, the overlap factor is enhanced in the region $X \gtrsim |\xi_M|$ with respect to the NI phase. These observations will help us to better understand the subsequent physics.

Results.—The imaginary part of the polarization function is calculated from Eq. (4), by employing the relation $\text{Im}[1/(\omega + i0^+)] = -\pi\delta(\omega)$. The real part is then obtained by the Kramers-Kronig relation. In Fig. 2 we plot $\Pi^R(X, \Omega)$ for $\xi_M = \xi_D = 0$. The imaginary part in Fig. 2(a) is strictly zero below the cutoff frequency Ω_{\min} , where electronic excitations are forbidden by energy-momentum conservation. In the Dirac limit ($X, \Omega \rightarrow 0$), the cutoff frequency is $\Omega_{\min} = X$, where a divergent behavior is observed [24] because the linear spectrum allows for the existence of a divergent number of particle-hole excitations satisfying the energy-momentum conditions. In the opposite limit ($X, \Omega \rightarrow \infty$), the polarization function goes to zero, due to the vanishing overlap factor, as expected in the 2DEG limit. At fixed X and $\Omega \rightarrow \infty$, the imaginary part decays as Ω^{-2} , while in a purely Dirac system it shows a Ω^{-1} decay. Whereas in graphene within RPA the real part of Π^R is always negative, for the BHZ model, as shown in Fig. 2(b), $\text{Re}[\Pi^R]$ changes sign and becomes positive in the region above Ω_{\min} indicated by the green dashed line. In this antiscreening region, we can search for solutions to Eq. (7), describing plasmonic resonances. Yet, Landau damping of the plasmon mode by single-particle excitation processes can be expected due to the finite value of $\text{Im}[\Pi^R]$ in the same region.

In Fig. 2(c), we plot line cuts of $\text{Im}[\Pi^R]$ for fixed $X = 0.5$ with and without ξ_D . A finite ξ_D strongly changes the polarization for small X , as $\text{Im}[\Pi^R]$ goes to zero at Ω_{\min} , instead of exhibiting the divergency known from graphene. This is due to the breaking of particle-hole symmetry and greatly diminishes the Landau damping of plasmons. In Fig. 2(d), we plot line cuts of $\text{Re}[\Pi^R]$ for fixed $X = 2$ and different Dirac masses. One nicely sees that, due to their effect on the overlap factor, a negative (positive) mass enhances (diminishes) the features of the polarization function with respect to the $M = 0$ case. Therefore, in a topologically nontrivial phase the antiscreening ($\text{Re}[\Pi^R] > 0$ part) effect gets enhanced, which increases the chance of observing plasmons.

Plasmons.—Now, we look for solutions of Eq. (7) corresponding to plasmon quasiparticles of definite energy

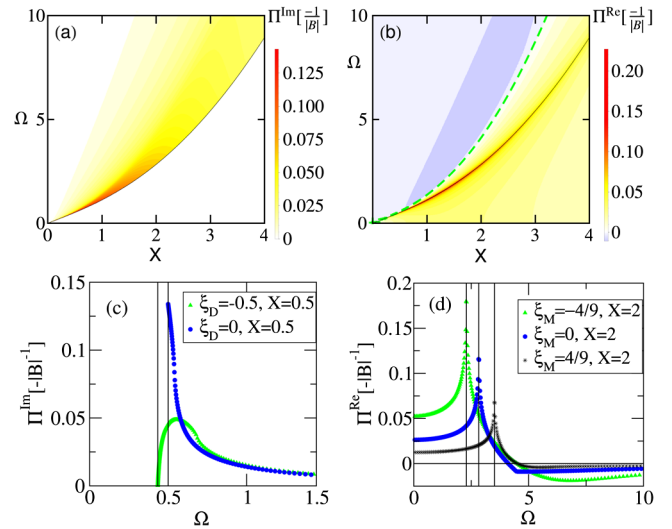


FIG. 2 (color online). Real (a) and imaginary (b) part of $\Pi^R(X, \Omega)$ of the BHZ model for $\xi_M = \xi_D = 0$. In (c) line cuts are drawn of $\text{Im}[\Pi^R]$ for $X = 0.5$, with $\xi_D = -0.5, 0$. The line cuts in (d) show $\text{Re}[\Pi^R]$ for $X = 2$ with $\xi_M = -4/9, 0$, and $4/9$, with green triangles, blue dots, and black stars, respectively.

and momentum (where $\Gamma/\Omega < 1$). For this purpose, Eq. (7) is expanded up to order $(\Gamma/\Omega)^2$ [14,31], resulting in two equations for the real and imaginary parts, from which we obtain the plasmon dispersion and its damping factor, respectively. We find that the damping ratio Γ/Ω parametrically depends on ξ_M and ξ_D only, but not on the interaction strength α . This behavior implies that Landau damping is due to the noninteracting single-particle excitations. In Fig. 3(a), we plot the damping ratio Γ/Ω for a TI phase with $\xi_M = -4/9$. For frequencies $\Omega \gg \Omega_{\min}$, the system is sufficiently undamped and the expansion in Γ/Ω is justified. In Fig. 3(b), we show the contour plot of $(\text{Re}[g(X, \Omega - i\Gamma)])^{-1}$ for $\xi_M = -4/9$. The isolines $(\text{Re}[g(X, \Omega - i\Gamma)])^{-1} = \alpha$ yield the plasmon dispersion curve for different interaction strength α . The plasmon dispersion relation has a square-root dependence on X , known from doped graphene [13] and ordinary 2DEG, for $\alpha \rightarrow \infty$, but shows instead an almost linear dependence (for small X) in the limit of $\alpha \rightarrow 0$. Plasmons are also revealed as peaks in the loss function $\text{Im}[-(1/\epsilon)]$. In Fig. 3(c) we compare the plasmon dispersion calculated from Eq. (7) with the loss function for an interaction strength of $\alpha = 0.4$ and $\xi_D = -0.5$. Evidently, plasmons are easily resolved and in perfect agreement with our analytical calculation. This is the key results of this Letter: the interplay between Dirac and Schrödinger fermions leads to a plasmonic excitation, which is absent in the limiting cases of a pure Dirac or Schrödinger system.

In Fig. 3(d), we plot the plasmon frequency and damping as a function of α at fixed $X = 0.5$ for a NI and a TI phase ($\xi_D = 0$) as well as for $\xi_D = -0.5$. As the plasmon frequency increases with α , for $\alpha \rightarrow \infty$ the damping ratio

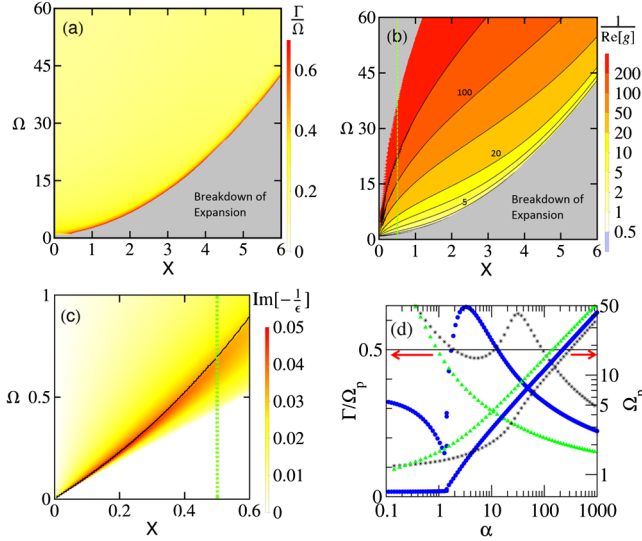


FIG. 3 (color online). (a) Illustration of the damping ratio Γ/Ω and (b) the function $1/\text{Re}[g(X, \Omega - i\Gamma)]$, for $\xi_M = -4/9$. (c) Plasmon dispersion together with the loss function $\text{Im}[-1/\epsilon]$ for $\xi_D = -0.5$ and $\alpha = 0.4$. (d) Plasmon frequency and damping at $X = 0.5$ [dashed line in (b) and (c)] for $\xi_M \in \{-4/9, 4/9\}$ and $\xi_D = -0.5$ in green triangles, black stars, and blue dots, respectively.

Γ/Ω_p decreases to values below $\Gamma/\Omega_p \lesssim 0.2$. Notably, at large α , the TI phase yields a larger plasmon frequency and is considerably less damped than the NI phase. This behavior directly stems from the enhancement of the antiscreening region of the polarization function due to the overlap factor enhancement in the TI phase. In the opposite limit, $\alpha \rightarrow 0$, the excessive damping leads to a breakdown of our expansion. For finite ξ_D , on the other hand, the plasmon damping has a minimum around $\alpha \approx 1$, which prevails to even smaller interaction strengths. This behavior is a direct consequence of the smaller $\text{Im}[\Pi^R]$ leading to reduced Landau damping for small plasmon frequencies.

Experimental realization.—Considering experimental parameters for Hg(Cd)Te structures [9,29], one finds roughly $\xi_D \leq -0.5$, $q_0 \approx 0.4 \text{ nm}^{-1}$, $E_0 \approx 140 \text{ meV}$, and masses M with absolute values up to several meV. The interaction strength is about $\alpha \approx 0.27$, resulting from $\alpha \approx 4/\epsilon_r$ with an average $\epsilon_r = 15$ from the CdTe substrate ($\epsilon_r = 10$) and HgTe ($\epsilon_r = 20$). As recently reported for the surface states of a 3D TI [21], plasmons with a ratio of $\Gamma/\Omega_p = 0.5$ are still observable in experiments. From Fig. 3 (d) we find $\Gamma/\Omega_p \approx 0.3$ for $\alpha \approx 0.27$ and $\xi_D = -0.5$. The wave vector and frequency of the plasmon are extracted from Fig. 3(c) to be $q \in [0.1, 0.6]q_0 = [0.04, 0.24] \text{ nm}^{-1}$ and $\omega \in [0.1, 0.8](E_0/\hbar) = [21, 170] \text{ THz}$, respectively, where the lower bound stems from the merging of plasmon and single-particle background for $X, \Omega \rightarrow 0$. This momentum and frequency range is of the right order for experimental techniques like Raman spectroscopy [32]. A finite

temperature in experiments can lead to doping by thermal excitations. At the temperature of liquid helium, one finds $k_B T_{\text{He}} \approx 0.35 \text{ meV}$, with k_B the Boltzmann constant. Thus, the plasmons resulting from thermal excitations occur on an energy and momentum scale at least 2 orders of magnitude smaller than the plasmons discussed in this Letter, making it possible to fully separate them or to suppress them with a small gap $k_B T < |M|$. We conclude that the plasmonic resonances discussed above are measurable, e.g., with Raman spectroscopy on Hg(Cd)Te quantum wells.

Optical conductivity.—From the knowledge of the polarization function, we can calculate the bulk optical conductivity of the system, defined by [33]

$$\sigma_0(\Omega) = \lim_{X \rightarrow 0} \frac{\Omega}{X^2} |B| \Pi^R(X, \Omega). \quad (9)$$

Notably, σ_0 is a universal function depending only on Ω and ξ_M . An analytical calculation yields

$$\text{Im}[\sigma_0(\Omega)] = - \left[\frac{1}{W} + \frac{1 + 4\xi_M}{\Omega^2} \left(\frac{1 + 2\xi_M}{W} - \frac{1}{2} \right) \right] \Theta(\Omega - 2|\xi_M|),$$

where $W = 2\sqrt{1 + 4\xi_M + \Omega^2}$.

In Fig. 4, we plot $\text{Im}[\sigma_0(\Omega)]$ for the different masses $\xi_M = -4/9, 0$, and $4/9$. Compared to the massless case, both positive and negative Dirac mass lead to a peak just above $\Omega_{\min} = 2|\xi_M|$. The signal from the TI phase is much stronger, diverging for $|\xi_M| \rightarrow 1/2$, which is the threshold of turning the band structure into a Mexican hat shape. Such difference between the trivial and topological phases is emphasized in the inset of Fig. 4, where we plot the ratio $R = \text{Im}[\sigma_0(\Omega)]_{M>0} / \text{Im}[\sigma_0(\Omega)]_{M<0}$. This behavior can be explained by considering the combined effects of the overlap factor and the phase space for the excitation process. In the TI phase of the BHZ model, the conduction and valence bands flatten for $X < |\xi_M|$, with respect to the NI phase. This fact enormously increases the number of finite momentum states available for an excitation just

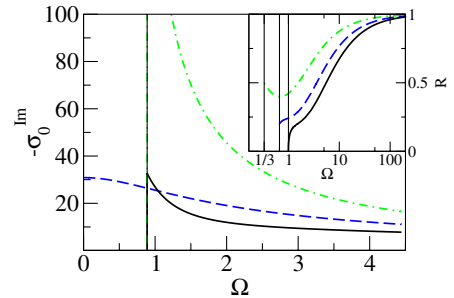


FIG. 4 (color online). Illustration of $\text{Im}[\sigma_0(\Omega)]$ for $\xi_M = -4/9, 0$, and $4/9$, with dot-dashed, long dashed, and solid lines, respectively. The inset shows the ratio $R = \text{Im}[\sigma_0(\Omega)]_{M>0} / \text{Im}[\sigma_0(\Omega)]_{M<0}$ for $|\xi_M| = 1/6, 1/3$, and $1/2$ in dot-dashed, long dashed, and solid lines, respectively.

above $\Omega_{\min} = |2\xi_M|$. The optical conductivity also shows a qualitatively different behavior as a function of $|\xi_M|$. Indeed, $\text{Im}[\sigma_0(\Omega)]$ increases (decreases) with increasing $|\xi_M|$ for a negative (positive) mass.

To conclude, we have analyzed the influence of Coulomb interaction—within RPA—on a mixed Dirac or Schrödinger fermion system described by the BHZ model. This model well describes a 2D TI realized in Hg(Cd)Te quantum wells. In the intrinsic limit, we could find observable plasmon solutions, which is a remarkable consequence of the peculiar electronic spectrum of the model. These plasmons occur for parameters suitable for experiments (like Raman spectroscopy) on Hg(Cd)Te quantum wells. Furthermore, we have predicted that a measurement of the optical conductivity at finite frequency (to be precise, above $\Omega = |2\xi_M|$) yields a direct way to distinguish between the two topological phases of Hg(Cd)Te quantum wells.

We acknowledge interesting discussions with M. Polini and financial support by the DFG (SPP1666 and the DFG-JST research unit *Topotronics*) as well as the Helmholtz Foundation (VITI).

-
- [1] A. K. Geim and K. S. Novoselov, *Nat. Mater.* **6**, 183 (2007).
 [2] A. H. Castro Neto, F. Guinea, N. M. R. Peres, K. S. Novoselov, and A. K. Geim, *Rev. Mod. Phys.* **81**, 109 (2009).
 [3] L. Fu and C. L. Kane, *Phys. Rev. B* **76**, 045302 (2007).
 [4] D. Hsieh, D. Qian, L. Wray, Y. Xia, Y. S. Hor, R. J. Cava, and M. Z. Hasan, *Nature (London)* **452**, 970 (2008).
 [5] M. Z. Hasan and C. L. Kane, *Rev. Mod. Phys.* **82**, 3045 (2010).
 [6] X.-L. Qi and S.-C. Zhang, *Rev. Mod. Phys.* **83**, 1057 (2011).
 [7] M. König, S. Wiedmann, C. Brüne, A. Roth, H. Buhmann, L. W. Molenkamp, X.-L. Qi, and S.-C. Zhang, *Science* **318**, 766 (2007).
 [8] B. A. Bernevig, T. L. Hughes, and S.-C. Zhang, *Science* **314**, 1757 (2006).
 [9] B. Büttner, C. X. Liu, G. Tkachov, E. G. Novik, C. Brüne, H. Buhmann, E. M. Hankiewicz, P. Recher, B. Trauzettel, S. C. Zhang, and L. W. Molenkamp, *Nat. Phys.* **7**, 418 (2011).
 [10] K. W.-K. Shung, *Phys. Rev. B* **34**, 979 (1986).
 [11] T. Ando, *J. Phys. Soc. Jpn.* **75**, 074716 (2006).
 [12] Y. Barlas, T. Pereg-Barnea, M. Polini, R. Asgari, and A. H. MacDonald, *Phys. Rev. Lett.* **98**, 236601 (2007).
 [13] E. H. Hwang and S. Das Sarma, *Phys. Rev. B* **75**, 205418 (2007).
 [14] B. Wunsch, T. Stauber, F. Sols, and F. Guinea, *New J. Phys.* **8**, 318 (2006).
 [15] V. N. Kotov, B. Uchoa, V. M. Pereira, F. Guinea, and A. H. Castro Neto, *Rev. Mod. Phys.* **84**, 1067 (2012).
 [16] A. N. Grigorenko, M. Polini, and K. S. Novoselov, *Nat. Photonics* **6**, 749 (2012).
 [17] T. Stauber, arXiv:1310.4296.
 [18] L. Ju, B. Geng, J. Horng, C. Girit, M. Martin, Z. Hao, H. A. Bechtel, X. Liang, A. Zettl, Y. R. Shen, and F. Wang, *Nat. Nanotechnol.* **6**, 630 (2011).
 [19] Z. Fei, A. S. Rodin, G. O. Andreev, W. Bao, A. S. McLeod, M. Wagner, L. M. Zhang, Z. Zhao, M. Thiemens, G. Dominguez, M. M. Fogler, C. A. H. Neto, C. N. Lau, F. Keilmann, and D. N. Basov, *Nature (London)* **487**, 82 (2012).
 [20] J. Chen, M. Badioli, P. Alonso-Gonzalez, S. Thongrattanasiri, F. Huth, J. Osmond, M. Spasenovic, A. Centeno, A. Pesquera, P. Godignon, E. A. Zurutuza, N. Camara, F. J. G. de Abajo, R. Hillenbrand, and F. H. L. Koppens, *Nature (London)* **487**, 77 (2012).
 [21] P. Di Pietro, M. Ortolani, O. Limaj, A. Di Gaspare, V. Giliberti, F. Giorgianni, M. Brahlek, N. Bansal, N. Koirala, S. Oh, P. Calvani, and S. Lupi, *Nat. Nanotechnol.* **8**, 556 (2013).
 [22] O. Vafek, *Phys. Rev. Lett.* **97**, 266406 (2006).
 [23] S. Das Sarma and Q. Li, *Phys. Rev. B* **87**, 235418 (2013).
 [24] S. Gangadharaiah, A. M. Farid, and E. G. Mishchenko, *Phys. Rev. Lett.* **100**, 166802 (2008).
 [25] I. Sodemann and M. M. Fogler, *Phys. Rev. B* **86**, 115408 (2012).
 [26] L. Brey and H. A. Fertig, *Phys. Rev. B* **75**, 125434 (2007).
 [27] C. L. Kane and E. J. Mele, *Phys. Rev. Lett.* **95**, 226801 (2005).
 [28] In order to have a band structure with a minimum at the Γ point, we restrict ourselves to masses $M > -(1/2)(A^2/|B|)$.
 [29] M. J. Schmidt, E. G. Novik, M. Kindermann, and B. Trauzettel, *Phys. Rev. B* **79**, 241306 (2009).
 [30] G. Giuliani and G. Vignale, *Quantum Theory of the Electron Liquid* (Cambridge University Press, Cambridge, England, 2008).
 [31] A. L. Fetter and J. D. Walecka, *Quantum Theory of Many-Particle Systems* (McGraw-Hill, New York, 1971).
 [32] J. Geurts (private communication).
 [33] F. Stern, *Phys. Rev. Lett.* **18**, 546 (1967).